Consistency of photon strength function models with data from the ^{94}Mo($d, p\gamma\gamma$) reaction

M. Krtička,[1] M. Wiedeking,[2] F. Bečvář,[1] and S. Valenta[1]
[1]*Faculty of Mathematics and Physics, Charles University, V Holešovičkách 2, Prague 8, Czech Republic*
[2]*iThemba LABS, P.O. Box 722, 7129 Somerset West, South Africa*
(Received 15 March 2016; published 9 May 2016)

Recently published study on the γ-ray energy dependence of photon strength functions (PSFs) from the population of ^{95}Mo low-lying levels in the ^{94}Mo$(d, p\gamma\gamma)^{95}$Mo reaction set out to answer some important questions related to the PSFs below the neutron separation energy in the Mo region. In this paper we discuss in detail actual relations of the quantities measured in this reaction to the PSFs and check the consistency of several available PSF models with experimental data. A broad variety of models was found to be consistent with experimental data at low E_γ. Although the photon strength very likely increases with decreasing energy at $E_\gamma \lesssim 3$ MeV, the data are unable to clearly differentiate whether the decrease follows the shape proposed from Oslo-type experiments or predictions of the generalized Lorentzian $E1$ model. The PSF shape at energies of 5–7 MeV is steeper than predicted by any standard model.

DOI: 10.1103/PhysRevC.93.054311

I. INTRODUCTION

Nuclear properties of medium-weight and heavy nuclei at excitation energies well above the pairing gap are believed to be best described with the statistical model of the nucleus. Within this model the ability of nuclei to emit or absorb photons with energy E_γ can be described by the nuclear level density (NLD) and the photon strength functions (PSFs) $f_{(XL)}(E_\gamma)$ for different types X (electric $X \equiv E$ or magnetic $X \equiv M$) and multipolarities L. Full understanding of these quantities is important, especially for the description of fuel cycles [1] and astrophysical element formation [2,3].

Until recently, data on PSFs in Mo isotopes in the low-energy region were available only from (^{3}He, ^{3}He$'\gamma$) and (^{3}He ,$\alpha\gamma$) Oslo-type experiments [4,5], (n,γ) reaction [6–8], and (γ,γ') experiments [9–11]. However, these data, as a whole, are inconsistent. A strong low-energy enhancement of the PSF (at $E_\gamma \lesssim 3$ MeV) was reported in charged-particle-induced γ-ray-production experiments analyzed with the so-called Oslo method [4]. However, results from the analysis of coincidence γ spectra from radiative neutron capture in even-even Mo isotopes indicated that this enhancement is weak, if at all present, and the data are consistent with predictions from the widely used generalized Lorentzian (GLO) model for $f_{(E1)}(E_\gamma)$ [12]. No restrictions on PSFs can be made from (γ,γ') at these energies. At higher energies ($E_\gamma \gtrsim 4$ MeV), there is a striking disagreement between PSFs from (γ,γ') and ^{3}He-induced experiments in even-even Mo isotopes [4,9]; see also comparison in Refs. [8,13]. Sensitivity of (n,γ) data to this E_γ region is restricted but models assuming PSF shape similar to that from ^{3}He-induced experiments seem to reproduce (n,γ) data successfully [6–8].

Experimental information on the XL composition of the PSF is available from intensities of primary transitions from (n,γ) reactions which yield $f_{(E1)}(E_\gamma)/f_{(M1)}(E_\gamma) \approx 4$ at $E_\gamma \approx 7$ MeV in Mo nuclei [14]. However, the composition is highly uncertain for lower E_γ. Theoretical predictions on the low-energy PSF enhancement observed in Oslo-type experiments exists for both $E1$ [15] and $M1$ [16] character in Mo nuclei. Analysis of coincidence spectra from (n,γ) reactions indicated $f_{(E1)}(E_\gamma) \approx f_{(M1)}(E_\gamma)$ in even-even Mo nuclei [6,7] at $E_\gamma \approx 3$–4 MeV.

Several years ago some of us published completely independent results on the E_γ dependence of PSFs from the analysis of ^{94}Mo$(d, p\gamma\gamma)$ data [17] measured with the STARS/LiberACE detector setup [18]. The E_γ dependence was obtained from inspecting the feeding of individual low-lying levels L_j with energies E_{L_j} in ^{95}Mo via a single γ ray from full sets of initial levels, residing in narrow intervals centered around initial excitation energies E_i; see Fig. 1. The energy E_i and particle identification were deduced from proton energies measured in $\Delta E - E$ telescopes. The feeding intensity $N_{L_j}(E_i, E_\gamma = E_i - E_{L_j})$ of levels L_j from energies around E_i via a single transition was obtained from considering all γ-γ coincidence events for which (i) a known γ-ray transition deexcites a well-resolved low-lying level L_j and (ii) the energy of the second γ ray is equal to $(E_i - E_{L_j})$ with 200-keV precision provided by the resolution of the $\Delta E - E$ telescopes; γ rays were measured with five high-purity germanium clover detectors. It was assumed that the emission of γ transitions with energies $E_\gamma \leqslant 400$ keV from initial energies near E_i is negligible; the justifiability of this assumption was verified with simulations within the statistical approach.

From various initial energies E_i, the feeding intensities $N_{L_j}(E_i, E_\gamma)$ to 13 low-lying levels with energies E_{L_j} (given in keV together with level spins J_{L_j} and parities) 204 $(3/2^+)$, 766 $(7/2^+)$, 786 $(1/2^+)$, 821 $(3/2^+)$, 948 $(9/2^+)$, 1039 $(1/2^+)$, 1074 $(7/2^+)$, 1370 $(3/2^+)$, 1426 $(3/2^+)$, 1552 $(9/2^+)$, 1620 $(3/2^+)$, 1660 $(3/2^+)$, and 3043 $(3/2^+)$ were extracted and for statistical reasons collected in 1-MeV-wide bins. The intensities $N_{L_j}(E_i, E_\gamma)$ for levels L_j with the same spin J_{L_j} could be exploited for determining the E_γ dependence of the PSF [17].

The outlined technique allows for a model-independent determination of the E_γ dependence of the PSF assuming that

$$N_{L_j}(E_i, E_\gamma)/E_\gamma^3 \propto f_{(E1)}(E_\gamma) + f_{(M1)}(E_\gamma). \quad (1)$$

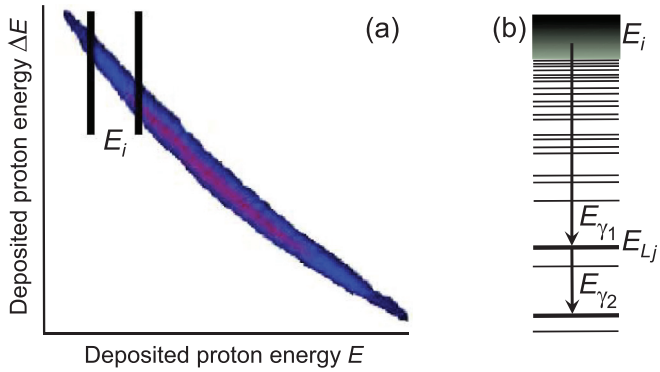

FIG. 1. Illustration of the procedure for determining intensities $N_{L_j}(E_i,E_{\gamma_1})$: (a) The proton energy deposited in $\Delta E - E$ telescopes determines the excitation energy E_i of the ^{95}Mo nucleus populated in the ^{94}Mo(d,p) reaction. (b) Additional coincidence of two γ rays—primary γ ray with $E_{\gamma_1} = E_i - E_{L_j}$ and a secondary γ ray with E_{γ_2}—which is known to deexcite a low-lying level at E_{L_j}, is required to validate the event.

However, the actual relation of the observables $N_{L_j}(E_i,E_\gamma)$ to the PSF and its XL characteristics have not been discussed in detail in Ref. [17]. This discussion is made in Sec. II of the present paper.

Assuming the validity of the above-mentioned simple relation between $N_{L_j}(E_i,E_\gamma)$ and PSF E_γ dependence, experimental data from the ^{94}Mo$(d,p\gamma\gamma)$ reaction were compared only to the PSF deduced from the ^{96}Mo(^{3}He ,$\alpha\gamma$) reaction [4] in Ref. [17]. A satisfactory agreement was found at least at low E_γ. Nevertheless, a detailed investigation of the consistency between $(d,p\gamma\gamma)$ experimental data and other PSF models has not been made so far. Comparisons with other PSF shapes, which mainly come from other experimental data on Mo nuclei, are presented in Sec. III. Main conclusions are then summarized in Sec. IV.

II. RELATION BETWEEN EXPERIMENTAL OBSERVABLES AND PHOTON STRENGTH FUNCTIONS

Only positive-parity levels L_j were studied in ^{95}Mo. Assuming that only $E1$ and $M1$ transitions are of importance—the role of higher multipolarities is expected to be negligible—intensities $N_{L_j}(E_i,E_\gamma)$ observed in the $(d,p\gamma\gamma)$ experiment are proportional to

$$N_{L_j}(E_i,E_\gamma) \propto \sum_{\substack{k,J \\ \pi_k=-}} \frac{\sigma^{(-)}_{kJ,(d,p)}(E_i)\Gamma^{(-)}_{kJ,(E1)}(E_i)}{\Gamma^{(-)}_{T,kJ}(E_i)} + \sum_{\substack{k,J \\ \pi_k=+}} \frac{\sigma^{(+)}_{kJ,(d,p)}(E_i)\Gamma^{(+)}_{kJ,(M1)}(E_i)}{\Gamma^{(+)}_{T,kJ}(E_i)}. \quad (2)$$

Here $\sigma^{(\bullet)}_{kJ,(d,p)}(E_i)$, $\Gamma^{(\bullet)}_{kJ,(XL)}(E_i)$, and $\Gamma^{(\bullet)}_{T,kJ}(E_i)$ are the cross section for the production of an individual level k with spin J in the excitation energy region near E_i in the (d,p) reaction, partial radiation width for the decay of level k to a low-lying level L_j, and total radiation width of the level k, respectively. The $\bullet$ symbol stands for positive (+) or negative (−) parity of the states at E_i. The sums in Eq. (2) go over all levels k in a 1-MeV-wide region centered around excitation energy E_i with the specified parity and over all spins J, which could feed a L_j level directly via a dipole γ transition. Of course, relations of the same type are valid not only for data from the (d,p) reaction, but for any other nuclear reaction when substituting the (d,p) cross section with the appropriate measure for production of levels k.

Individual values of all involved quantities fluctuate around their expectation values. The expectation value of the average partial radiation width of levels at E_i with spin J and parity $\bullet$, $\overline{\Gamma}^{(\bullet)}_{J,(XL)}(E_i)$ can further be expressed as [19]

$$\overline{\Gamma}^{(\bullet)}_{J,(XL)}(E_i) = f_{(XL)}(E_\gamma)E^3_\gamma/\rho^{(\bullet)}_J(E_i), \quad (3)$$

where $\rho^{(\bullet)}_J(E_i)$ is the density of nuclear levels with spin J and parity $\bullet$ at E_i.

Combining Eqs. (2) and (3) we get

$$N_{L_j}(E_i,E_\gamma)/E^3_\gamma \propto w^{(-)}(E_i)f_{(E1)}(E_\gamma) + w^{(+)}(E_i)f_{(M1)}(E_\gamma), \quad (4)$$

where we defined $w^{(\bullet)}(E_i)$ as

$$w^{(\bullet)}(E_i) = \sum_J \frac{\overline{\sigma}^{(\bullet)}_{J,(d,p)}(E_i)}{\overline{\Gamma}^{(\bullet)}_{T,J}(E_i)\rho^{(\bullet)}_J(E_i)} F^{(\bullet)}_J = \sum_J \overline{w}^{(\bullet)}_J(E_i)F^{(\bullet)}_J, \quad (5)$$

with factor $F^{(\bullet)}_J$ describing the combined fluctuation of involved quantities. Quantities $\overline{\sigma}^{(\bullet)}_{J,(d,p)}(E_i)$ and $\overline{\Gamma}^{(\bullet)}_{T,J}(E_i)$ are the average (d,p) reaction cross section populating levels at E_i with spin J and parity $\bullet$ and average total radiation width of these states. The discussion of fluctuation properties of $w^{(\bullet)}(E_i)$, which are important for the quantitative description of an agreement between data and PSF model predictions, will be made in Sec. III B. Here let us concentrate on the relation between $N_{L_j}(E_i,E_\gamma)$ and expectation values $\overline{w}^{(\bullet)}_J(E_i)$. To simplify the discussion, the possible J dependence of $\overline{w}^{(\bullet)}_J(E_i)$ is not considered explicitly, but it will only be commented on in specific cases. Omitting this spin dependence, we can write

$$N_{L_j}(E_i,E_\gamma)/E^3_\gamma \propto f_{(E1)}(E_\gamma) + \frac{\overline{w}^{(+)}(E_i)}{\overline{w}^{(-)}(E_i)} f_{(M1)}(E_\gamma), \quad (6)$$

where the factor $\overline{w}^{(+)}(E_i)/\overline{w}^{(-)}(E_i)$ depends on excitation energy E_i.

Observables $N_{L_j}(E_i,E_\gamma)$ yield clear information on the PSF only if $\overline{w}^{(+)}(E_i) \approx \overline{w}^{(-)}(E_i)$; the observed E_γ dependence of $N_{L_j}(E_i,E_\gamma)/E^3_\gamma$ is then proportional to $f_{(E1)}(E_\gamma) + f_{(M1)}(E_\gamma)$. As becomes evident from the following discussion, a strong dominance of one transition type (electric or magnetic) does not guarantee that $N_{L_j}(E_i,E_\gamma)/E^3_\gamma$ is proportional to the PSF for this type.

Realizing that the total radiation width $\Gamma^{(\bullet)}_{T,J}(E_i)$ is the sum of partial radiation widths for transitions to all levels f with excitation energy $E_f < E_i$, the product $\overline{\Gamma}^{(\bullet)}_{T,J}(E_i)\rho^{(\bullet)}_J(E_i)$ can

be, using Eq. (3), rewritten as

$$\overline{\Gamma}^{(\bullet)}_{T,J}(E_i)\rho^{(\bullet)}_J(E_i) = \sum_{\substack{f \\ \pi_i \neq \pi_{L_j}}} f_{(E1)}(E_\gamma)E_\gamma^3 + \sum_{\substack{f \\ \pi_i = \pi_{L_j}}} f_{(M1)}(E_\gamma)E_\gamma^3. \quad (7)$$

The quantity $\overline{\Gamma}^{(\bullet)}_{T,J}(E_i)$, as well as the product on the left-hand side of Eq. (7), are difficult to obtain from existing experimental data at excitation energies E_i of our interest. Therefore, we have to rely on simulations of these quantities within the statistical model. Such simulations, performed using the DICEBOX code [20], indicate that in ^{95}Mo the product $\overline{\Gamma}^{(\bullet)}_{T,J}(E_i)\rho^{(\bullet)}_J(E_i)$ from Eq. (7) can differ for levels with the same parity but different spin, as well as for levels with the same spin but opposite parity at a given E_i.

Clear examples of a significant dependence of $\overline{\Gamma}^{(\bullet)}_{T,J}(E_i)\rho^{(\bullet)}_J(E_i)$ on parity are low-E_i regions in nuclei with levels of only one parity near the bottom of the level scheme. This is the case in ^{95}Mo, where, below an excitation energy of about 2 MeV, there are only positive-parity levels. As a result, at excitation energy $E_i \approx 3$–5 MeV levels with positive (negative)-parity decay dominantly via $M1$ ($E1$) transitions. If $f_{(E1)}(E_\gamma) \gg f_{(M1)}(E_\gamma)$ at $E_\gamma \approx 2$–5 MeV and $\rho^{(+)}_J(E_i) \approx \rho^{(-)}_J(E_i)$ at $E_i \approx 3$–5 MeV, then $\overline{\Gamma}^{(-)}_{T,J}(E_i) \gg \overline{\Gamma}^{(+)}_{T,J}(E_i)$. Shell-model calculations of ^{95}Mo, presented in Ref. [21], indicated an independence of the NLD on parity above excitation energy of about 2.5 MeV. Assuming PSF of pure $E1$ character together with parity independence of NLD at initial energies, simulations with model combination B, which is based on Oslo data (see below), indicate that the ratio $\overline{\Gamma}^{(-)}_{T,J}(E_i)\rho^{(-)}_J(E_i)/\overline{\Gamma}^{(+)}_{T,J}(E_i)\rho^{(+)}_J(E_i)$ would be about 10, 4, and 2.5 for $E_i = 3$, 4, and 5 MeV, respectively. Such different values could easily lead to $\overline{w}^{(+)}(E_i) \gg \overline{w}^{(-)}(E_i)$; the dominance of $f_{(M1)}(E_\gamma)$ over $f_{(E1)}(E_\gamma)$ at $E_\gamma \approx 2$–5 MeV would lead to the opposite relation, i.e., $\overline{w}^{(-)}(E_i) \gg \overline{w}^{(+)}(E_i)$.

However, simulations with model combination A—a model for which we *a priori* know the XL composition and which reasonably describes ^{96,98}Mo(n,γ) data [6–8] (see below)—show that the ratio of the $\overline{\Gamma}^{(\bullet)}_{T,J}(E_i)\rho^{(\bullet)}_J(E_i)$ for levels with the same spin but opposite parity is much smaller and decreases from about 1.3 at $E_i \approx 3$ MeV down to about 1.2 at S_n, i.e., neutron resonances, being higher for negative-parity levels. Similar values of $\overline{\Gamma}^{(\bullet)}_{T,J}(E_i)$ for levels with both parities, at least for $E_i \lesssim 5$ MeV, result from comparable $f_{(E1)}(E_\gamma)$ and $f_{(M1)}(E_\gamma)$ at $E_\gamma \lesssim 5$ MeV. The experimental ratio of the average total radiation widths for p-wave (negative-parity) and s-wave (positive-parity) neutron resonances, i.e., levels near $E_i \approx 7.4$ MeV, is 1.46(13) [22].

Simulated differences in $\overline{\Gamma}^{(\bullet)}_{T,J}(E_i)$ on spin J for fixed E_i and parity $\bullet$ are up to about 1.7 and 2 for levels differing by one and two units of spin, respectively; the maximum value of $\overline{\Gamma}^{(\bullet)}_{T,J}(E_i)$ is reached for $J = 5/2$ levels. Nonetheless, the J dependence of $\overline{\Gamma}^{(\bullet)}_{T,J}(E_i)$ is not of great importance, as the difference is very similar for levels with both parities.

Similarly to $\overline{\Gamma}^{(\bullet)}_{T,J}(E_i)$, experimental data on spin and parity dependence of the cross section are not available for the E_i of interest. The average cross sections $\overline{\sigma}^{(\bullet)}_{J,(d,p)}(E_i)$ for the production of levels with different parities were calculated with the TALYS reaction code [23]. The calculations indicate that $\overline{\sigma}^{(+)}_{J,(d,p)}(E_i) \approx \overline{\sigma}^{(-)}_{J,(d,p)}(E_i)$ at all energies E_i relevant for our experiment. The calculated J dependence of $\overline{\sigma}_{J,(d,p)}(E_i)$ then scales nicely with the spin dependence of level density [21]. This latter dependence justifies the fact that we discussed only the spin dependence of $\overline{\Gamma}^{(\bullet)}_{T,J}(E_i)$ instead of $\overline{\Gamma}^{(\bullet)}_{T,J}(E_i)\rho^{(\bullet)}_J(E_i)$ in the previous paragraph, as the ratio $\overline{\sigma}^{(\bullet)}_{J,(d,p)}/\rho^{(\bullet)}_J(E_i)$ is expected to be virtually independent of spin J.

A combination of all findings discussed above indicates that $\overline{w}^{(+)}(E_i)/\overline{w}^{(-)}(E_i) \propto \overline{\Gamma}^{(-)}_{T,J}(E_i)/\overline{\Gamma}^{(+)}_{T,J}(E_i)$ for E_i, where the NLD is independent of parity; the ratio is at the same time virtually independent of J. The relation given in Eq. (1) is then valid only if $\overline{\Gamma}^{(+)}_{T,J}(E_i) \approx \overline{\Gamma}^{(-)}_{T,J}(E_i)$. This assumption seems to be closely matched to the real situation in ^{95}Mo. However, experimental data on $\Gamma_{T,\mathrm{res}}$, as well as results from simulations indicate that its validity is only approximate and that the E_γ dependence of the $M1$ PSF might be enhanced in the E_γ dependence of observables $N_{L_j}(E_i,E_\gamma)/E_\gamma^3$.

III. CONSISTENCY OF EXPERIMENTAL DATA WITH PSF MODELS

The discussion in the previous section indicates that the relation between the E_γ dependence of our observables $N_{L_j}(E_i,E_\gamma)/E_\gamma^3$ and the PSF might be very complicated, in general, but it should be close to $f_{(E1)}(E_\gamma) + f_{(M1)}(E_\gamma)$ in ^{95}Mo. We thus decided to investigate the compatibility of several PSF models with experimental data, assuming validity of Eq. (1). We were also able to investigate models where PSFs do not only depend on E_γ but also on excitation energy.

A. Tested PSFs models

Tested PSF models describe well experimental data from different reactions in ^{95}Mo or neighboring Mo nuclei. Specifically, we used (i) a model which well described two-step and multistep γ cascade data following slow neutron capture in the neighboring nucleus ^{96}Mo [6,7], (ii) the PSF shape reproducing data from the ^{96}Mo(^{3}He,$\alpha\gamma$)^{95}Mo reaction [4,24], and (iii) a model describing (γ,γ') data at $E_\gamma > 4$ MeV [9]. A couple of other models were also tested; see below. Strictly speaking, only some of the tested PSF shapes are based on theory and can be called models, while the others are based on fits to experimental data. Nevertheless, for the sake of brevity, all tested PSF shapes will be referred to as "models."

1. Models reproducing (n,γ) data

The PSF model reproducing (n,γ) data consisted of a generalized Lorentzian (GLO) model [12] for $f_{(E1)}(E_\gamma,T_f)$ and a combination of the Lorentzian spin-flip (SF) resonance and a single-particle (SP) strength for $f_{(M1)}(E_\gamma)$. The parameters

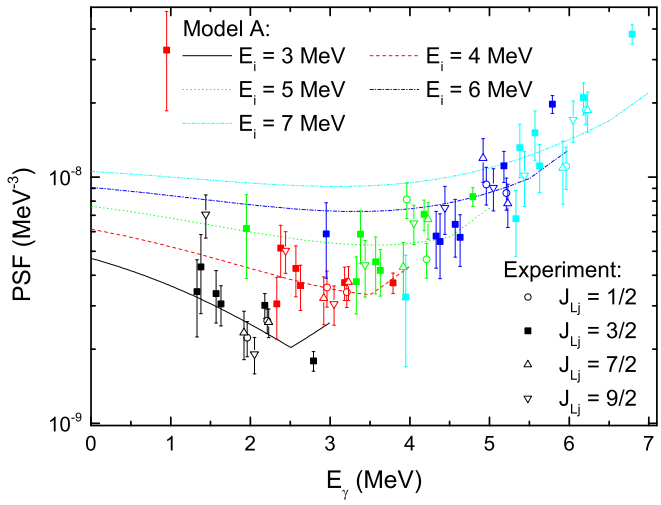

FIG. 2. Comparison of experimental $N_{L_j}(E_i,E_\gamma)/E_\gamma^3$ data with predictions of the PSF model describing (n,γ) data in ^{96}Mo (model A). Different colors of experimental data correspond to different E_i, in agreement with the model color coding; different symbols are used for different spins of L_j. Experimental data are normalized to corresponding modeled E_i curves.

of the giant electric dipole resonance (GEDR) adopted in our comparison were exactly those used in the analysis of ^{95}Mo(n,γ) data [6,7]; $E_{\rm GEDR} = 16.20$ MeV, $\Gamma_{\rm GEDR} = 6.01$ MeV, and $\sigma_{\rm GEDR} = 185$ mb [25]. The $f^{\rm GLO}_{(E1)}(E_\gamma,T_f)$ depends not only on E_γ but also on the temperature of the final level reached through γ decay $T_f = \sqrt{a(E_i - E_\gamma - \Delta)}$, where a is a level density parameter and Δ is a pairing energy; $a = 9.78$ MeV^{-1} was considered in our analysis [26]. There are several different approaches to how to treat Δ: (i) $\Delta = P_n = 1.33$ MeV for ^{95}Mo, where P_n is the neutron pairing energy in neutron-odd nuclei calculated from neutron separation energies of neighbor nuclei [27]; (ii) $\Delta = P_d = 0.49$ MeV for ^{95}Mo, where P_d is the deuteron pairing energy [26]; and (iii) $\Delta = C_1 + P_n$, where the backshift parameter $C_1 = -6.6A^{-0.32}$ [27] yields $\Delta = -0.2$ MeV in ^{95}Mo. The choice of Δ influences the PSF shape obtained from the GLO model. Hereafter, the symbols A, $A^\dagger$, and A^* will be used for the above-described PSF model combinations with $\Delta = 0.49$, -0.2, and 1.33 MeV adopted in the $f^{\rm GLO}_{(E1)}(E_\gamma,T_f)$ model, respectively. The PSF model combination A ($\Delta = 0.49$ MeV) is plotted in Fig. 2, together with experimental $N_{L_j}(E_i,E_\gamma)/E_\gamma^3$ data. A normalization of experimental data sets for each E_i and J_{L_j} is independent and made with respect to the corresponding calculated E_i curves.

All A-type model combinations (A, $A^\dagger$, A^*) are decreasing functions of E_γ at low energies. The slope of the decrease depends on E_i—the higher the E_i, the flatter is the PSF—and the minimum in the PSF is reached for $E_\gamma = E_i - \Delta$ for transitions from $E_i \lesssim 4.5$ MeV and is shifted to lower E_γ than given by $E_i - \Delta$ for higher E_i.

2. *Models reproducing Oslo data*

We tested PSF shapes which reproduce ^{96}Mo$(^3$He$,\alpha\gamma)^{95}$Mo data and were obtained from the analysis of experimental data using the Oslo method [4]. The simultaneous extraction of NLD and PSF using this method produces PSF uncertain by a factor e^{cE_γ}. The value of the constant c is usually determined from a fit of NLD to the number of low-lying levels and the density of neutron resonances [5,24]. Probably the most significant problem in determining constant c comes from uncertainties of the NLD spin dependence; the spin dependence is usually characterized by the spin cutoff parameter σ_c. This parameter is used to obtain total NLD in the neutron resonance region as the available measured data on neutron resonances cover only a narrow spin window, while data from ^{3}He-induced reactions correspond to a broad range of spins. In principle, using $(d,p\gamma\gamma)$ data, we might try to determine the value of c and further estimate what fraction of total NLD is represented by neutron resonances with given J^π (or equivalently determine σ_c).

TABLE I. Parameters of quadratic PSF fits $f(E_\gamma)$ [MeV^{-3}] $= 10^{-9}(a + bE_\gamma + cE_\gamma^2)$ adopted for models of B and D type. Energies E_γ are to be given in MeV. Two parameter sets for model D correspond to E_γ regions below and above 3.85 MeV.

Model	a	b	c
B	17.46	−8.176	1.225
B^*	17.11	−9.398	1.738
D ($E_\gamma < 3.85$ MeV)	14.05	−5.923	0.921
D ($E_\gamma > 3.85$ MeV)	74.84	−37.27	4.962

Two different normalizations for the ^{96}Mo$(^3$He$,\alpha\gamma)$ data [4,24], which differ in σ_c, were adopted. In practice, the experimental points, corresponding to these two normalizations, were approximated with quadratic fits. These quadratic fits are further labeled as models B (fit to normalization from Ref. [4]) and B^* (fit to normalization from Ref. [24]), with parameters of the fits listed in Table I. No information on the XL PSF makeup was derived directly from ^{3}He-induced data. Nevertheless, experimental data from angular correlation measurement in ^{56}Fe indicated that the PSF at low E_γ is dominantly of dipole nature [28].

The absolute normalizations of B-type models cannot be determined from experimental data. It is usually adjusted to reproduce the total radiation width of neutron resonances, $\Gamma_{T,\rm res}$. In our case, we fixed the normalization to reasonably reproduce data points for $E_\gamma \lesssim 5$ MeV presented in Fig. 3. Resulting B and B^* models are shown therein. The normalization of experimental data points in Fig. 3 is presented below; see Sec. III A 4.

3. *Models reproducing (γ,γ') data*

Experimental data from (γ,γ') are available for $E_\gamma >$ 4 MeV in even-even Mo isotopes from measurements at ELBE [9] and for ^{94}Mo and ^{98}Mo also from the HIγS facility [10,11]. The E_γ dependence of the PSF from ELBE measurements in this region is similar for $^{94-98}$Mo nuclei. For our purpose we approximated the (γ,γ') experimental points with the same E_γ dependence of the PSF as in the analysis of ^{98}Mo multistep cascade data [8] and labeled this

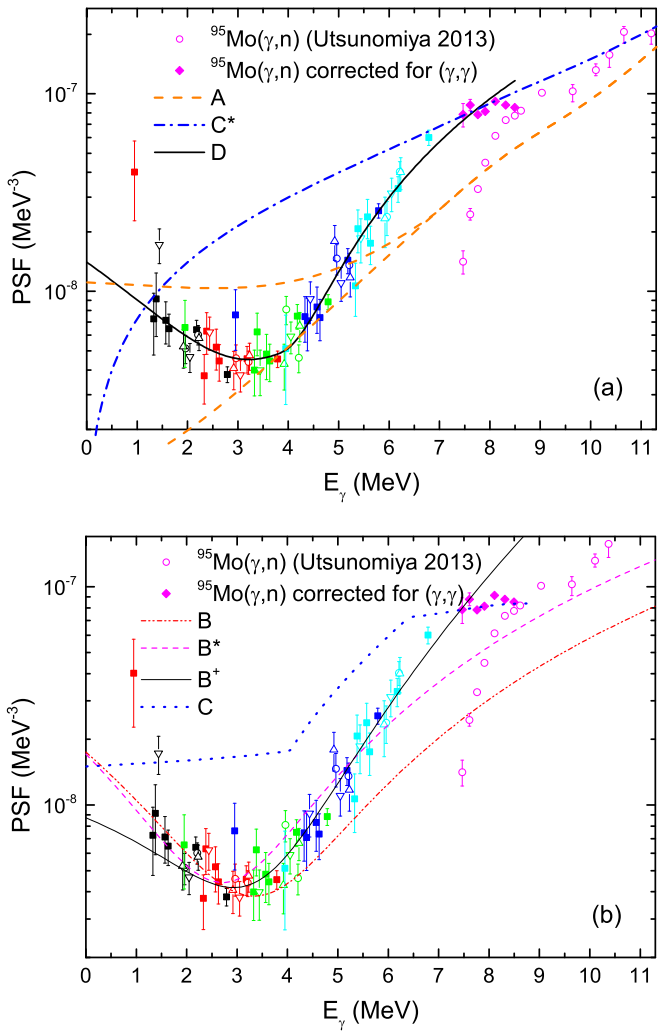

FIG. 3. Comparison of experimental data with tested PSF models; for details of the models, see the main text. Two curves in panel (a), corresponding to transitions from S_n (upper curve) and transitions to the ground state (lower curve) are plotted for model A, which depends on the excitation energy. Normalization of experimental data from each E_i and J_{L_j} is made with respect to model D in both panels of the figure. For a quantitative comparison of experimental data with predictions, individual normalization factors must be applied for each model and each pair of E_i and J_{L_j}. Symbols used for experimental data are the same as those in Fig. 2.

PSF shape as model combination C. Strictly speaking, the model combination can be tested only for $E_\gamma > 4$ MeV. However, we decided to extend the E_γ dependence of the model combination *ad hoc* below $E_\gamma = 4$ MeV, where no data from (γ,γ') are available, in line with the extension used in Ref. [8]; we used a constant $E1$ PSF in combination with the tail of the spin-flip $M1$ resonance. As a result, the PSF in model C is a slowly increasing function of E_γ below $E_\gamma = 4$ MeV.

HIγS data on Mo isotopes indicate that the E_γ dependence of the PSF could be similar to a Lorentzian shape [9,10]. Therefore, we decided to test also the Lorentzian $E1$ PSF shape in combination with the spin-flip $M1$ resonance and labeled this model combination as C^*. Model combinations of C type are plotted in Fig. 3. The normalization to γ absorption data above S_n was adopted for these models.

4. PSF dependence derived from $(d,p\gamma\gamma)$ data

Data on $N_{L_j}(E_i,E_\gamma)$ for $J_{L_j} = 3/2$ levels from different E_i display a significant overlap in γ-ray energy. We used this fact for constructing a PSF model exclusively from ^{94}Mo$(d,p\gamma\gamma)$ data assuming no E_i (or equivalently T_f) PSF dependence, in line with the Brink hypothesis [29]. To get the E_γ dependence of the PSF, we fitted $N_{L_j}(E_i,E_\gamma)/E_\gamma^3$ data independently from different E_i with a quadratic E_γ function. These fits for the three lowest initial regions, $E_i = 3$–5 MeV, show an almost identical E_γ dependence. As a result, the E_γ dependence between about 1 and 4 MeV seems to be well approximated with a simple quadratic function.

The E_γ dependence of individual quadratic fits for higher E_i start to deviate from one another. Nevertheless, we can match the fits for $E_i = 4$ MeV and $E_i = 6$ MeV at $E_\gamma = 3.85$ MeV, where these two fits display close values of their derivatives, to obtain a good approximation of $(d,p\gamma\gamma)$ experimental points over the whole measured E_γ interval. This bi-quadratic E_γ dependence is labeled as model D and is also plotted in Fig. 3. The parameters of quadratic fits used in this model are listed in Table I. At $E_\gamma \lesssim 4$ MeV the PSF shape is similar to predictions of the B and B^* models which are based on Oslo data. Similarly to B-type models, we are unable to make statements regarding the XL makeup of model D.

Absolute normalization of the D model is not possible from ^{94}Mo$(d,p\gamma\gamma)$ data. The normalization in Fig. 3 corresponds to reasonable matching of the model D to the total γ absorption cross section $\sigma_{\gamma T}$ just above S_n. In reality, to get $\sigma_{\gamma T}$ a significant correction of the (γ,n) data [30] for (γ,γ') contributions has to be made at energies between S_n and about 9 MeV, as neutrons emitted from states at these energies have to carry very high orbital momentum [21]. We tried to estimate the contribution of $\sigma_{\gamma\gamma'}$ to $\sigma_{\gamma T}$ with the TALYS code [23] using its default models. Deduced values of the PSF after this correction are shown in Fig. 3 as solid diamonds. The ^{94}Mo$(d,p\gamma\gamma)$ experimental data in both panels of Fig. 3 are then normalized with respect to the model D.

5. A constant PSF

Models of A, B, and D type show a decrease of PSF with increasing E_γ at $E_\gamma \lesssim 4$ MeV. It seems very interesting to check whether we really need any decrease in PSF at low E_γ. To test this, we also investigated a constant PSF for low E_γ and labeled it as model E.

B. Expected fluctuations of individual intensities

Factor $F_J^{(\bullet)}$ from Eq. (5) describes the influence of fluctuations of individual quantities on the right-hand side of Eq. (2) on $N_{L_j}(E_i,E_\gamma)$. Uncertainties owing to this factor should be added to experimental errors when quantifying the agreement between experimental data and PSF model predictions.

The statistical model assumes that individual partial radiation widths fluctuate around their expectation value with a

TABLE II. The χ^2 values characterizing the agreement of tested models with experimental data for five (1-MeV-wide) excitation energy regions of initial levels, labeled via midpoint energy E_i, and four values of spin J_{L_j} of final levels L_j. Values of $N(E_i)$ represent the expected number of levels, predicted by the CT and the BSFG NLD models, within the 1-MeV-wide interval centered around E_i, which can decay to final levels with spin J_{L_j} via dipole transitions. Quantity Σ_F represents the expected relative rms of the fluctuation of transitions from the 1-MeV-wide region around E_i to a low-lying level L_j; see Sec. III B. Values of ν give the number of degrees of freedom for each data set. The uncertainty used in the calculation of χ^2 values is a sum in quadrature of experimental errors and Σ_F.

E_i	J_{L_j}	$N(E_i)$		Σ_F (%)		ν	χ^2									
(MeV)		CT	BSFG	CT	BSFG		A	A^*	$A^\dagger$	B	B^*	$B^\dagger$	C	C^*	D	E
3.0	3/2	65	105	21	15	5	4.745	18.967	3.149	1.441	2.751	3.368	10.124	25.084	2.100	8.684
4.0	3/2	200	340	11	8	6	6.111	14.450	5.946	5.989	10.340	7.390	6.501	13.993	5.536	6.078
5.0	3/2	650	950	6	5	6	10.436	2.722	13.614	4.187	4.209	5.295	4.829	7.058	6.508	
6.0	3/2	1700	2300	4	3	6	31.210	15.444	36.823	11.609	12.168	3.802	10.857	31.691	2.476	
7.0	3/2	5300	5800	2	2	6	54.331	40.857	59.568	24.798	25.443	7.992	33.049	55.275	9.155	
3.0	1/2	35	60	28	21	1	0.541	0.028	0.385	0.666	0.547	0.414	0.170	0.007	0.505	0.198
4.0	1/2	110	180	15	11	1	0.001	0.392	0.008	0.000	0.180	0.061	0.048	0.253	0.012	0.026
5.0	1/2	350	530	8	6	1	4.926	6.662	4.927	6.118	6.964	7.101	6.528	5.735	6.875	
6.0	1/2	1100	1400	4	4	1	0.333	0.786	0.308	0.819	0.845	1.324	0.832	0.374	1.679	
7.0	1/2	3500	3600	2	2	1	3.963	3.086	4.070	3.180	3.308	2.240	3.291	4.299	2.371	
3.0	7/2	80	130	19	14	1	0.500	0.006	0.297	0.681	0.516	0.334	0.064	0.036	0.455	0.090
4.0	7/2	260	420	9	7	1	0.463	0.001	0.376	0.502	0.050	0.186	0.211	0.014	0.353	0.278
5.0	7/2	850	1300	5	4	1	1.951	0.839	1.949	1.138	0.700	0.646	0.992	1.361	0.772	
6.0	7/2	2700	3500	2	2	1	2.736	3.736	2.671	3.798	3.852	4.674	3.828	2.847	5.230	
7.0	7/2	8700	9000	2	2	1	1.818	1.318	1.880	1.369	1.440	0.858	1.431	2.009	0.924	
3.0	9/2	70	120	20	14	1	6.661	8.195	7.336	5.785	5.857	7.030	8.661	10.833	6.447	8.468
4.0	9/2	240	400	10	8	1	1.723	3.673	2.066	1.005	2.858	2.197	3.006	5.311	1.644	2.672
5.0	9/2	780	1150	5	4	1	1.431	0.387	1.376	0.607	0.021	0.083	1.179	0.383	0.373	
6.0	9/2	2500	3300	3	3	1	0.061	0.043	0.076	0.236	0.367	0.943	0.394	0.003	1.769	
7.0	9/2	8200	8500	2	2	1	1.214	0.629	1.306	0.383	0.441	0.016	0.453	1.346	0.009	

χ^2_ν distribution with $\nu = 1$ degree of freedom, the so-called Porter-Thomas distribution (PTD) [31].

Expected fluctuations of total radiation widths are significantly suppressed with respect to the PTD. As evident from Eq. (7), their size depends on the number and energy of final levels f below E_i. In general, they decrease with E_i as the accessible number of final levels f increases. They can be estimated for any combination of PSF and NLD models from statistical model simulations. Using the DICEBOX algorithm [20] we found that they do not significantly depend on spin and parity of a level at given E_i and they decrease with excitation energy from about 35% at $E_i = 3$ MeV to about 10%–15% at $E_i = 7$ MeV, slightly depending on the NLD and PSF models.

Fluctuation properties of $\sigma_{kJ,(d,p)}(E_i)$ are not well known. Within the strict version of the statistical approach they should be described by the PTD for each reaction channel, but actual fluctuations of $\sigma_{kJ,(d,p)}(E_i)$ might significantly differ from the PTD. Nevertheless, naive inspection of spectroscopic factors for levels at low excitation energies in ^{95}Mo from Ref. [32] indicates that the distribution of $\sigma_{iJ,(d,p)}(E_i)$ is not very narrow.

To test the compatibility of PSF models with experimental data, we could adopt different assumptions on fluctuations of $\sigma_{kJ,(d,p)}$. In reality, we decided to use two assumptions: (i) $\sigma_{kJ,(d,p)}(E_i)$ fluctuate according to the PTD and (ii) there is no fluctuation of $\sigma_{kJ,(d,p)}(E_i)$ at all. The former assumption is believed to be closer to reality, but the latter one was chosen to show that even this unrealistic assumption, which definitely underestimates the real fluctuations, allows for good consistency of a broad variety of tested PSF models with experimental data.

Expected rms values of relative fluctuations of $N_{L_j}(E_i, E_\gamma)$, labeled here as Σ_F, are determined by fluctuation properties of γ transitions from individual levels at E_i and the number of these levels. Unfortunately, the number of levels at E_i is not known. We decided to estimate this number with help of NLD models. For this purpose we adopted the back-shifted Fermi gas (BSFG) and the constant-temperature (CT) models [26]. The BSFG model predicts a higher number of levels than the CT model at excitation energies of interest, $E_i = 3$–7 MeV. The expected total numbers of levels $N(E_i)$ (of both parities) in a 1-MeV-wide interval around E_i, which can decay to levels with spin J_{L_j} by dipole transitions, for both these NLD models are listed in Table II.

Assuming that (i) there is no fluctuation in $\sigma_{kJ,(d,p)}(E_i)$ and (ii) levels with all spins and both parities contribute with the same weight $\overline{w}_f^{(\bullet)}(E_i)$ to the sum in Eq. (5), the Σ_F values are listed in Table II for both NLD models; the fluctuation of total radiation widths, mentioned earlier in this section, was considered in calculating the Σ_F values. Both of these assumptions make the presented values of Σ_F at most equal but more likely considerably smaller than the actual fluctuations. First, as mentioned above, individual $\sigma_{kJ,(d,p)}(E_i)$ are expected to fluctuate. Assuming the PTD for fluctuations of

$\sigma_{kJ,(d,p)}$, the listed Σ_F then increases by a factor of about 1.7. Second, any deviation of $f_{(E1)}(E_i - E_{L_j})/f_{(M1)}(E_i - E_{L_j})$ from unity discriminates contribution of levels with one parity to $N_{L_j}(E_i, E_\gamma)$ and effectively lowers the number of levels $N(E_i)$ which can decay to low-lying levels with spin J_{L_j} via dipole transitions; the values of Σ_F are proportional to $1/\sqrt{N(E_i)}$.

The Σ_F fluctuations were incoherently added to experimental uncertainties when testing the compatibility of PSF models with experimental data.

C. Results

The χ^2 values characterizing the agreement of tested PSF models with experiment are presented in Table II for individual initial energies E_i, spins of final levels J_{L_j}, and relative fluctuations Σ_F corresponding to the BSFG NLD model (sixth column of the table). The number of degrees of freedom ν, also given in Table II, corresponds to the number of available final levels L_j in ^{95}Mo with spin J_{L_j} decreased by one as there is an independent normalization factor between experiment and simulations for each E_i and J_{L_j}. Data sets for different E_i, as well as J_{L_j} are fully independent, which allows for easy checks of the consistency of predictions with experiment using different combinations of these data sets.

In reality, restrictions on the PSF E_γ dependence can be made almost exclusively only from $J_{L_j} = 3/2$ data sets. For all other spins, J_{L_j} information on intensities $N_{L_j}(E_i, E_\gamma)$ is available only for two levels with similar excitation energy E_{L_j}. Ratios of these intensities for levels with similar E_{L_j} should be close to unity. As a result, the χ^2 values obtained for these spins should serve rather for checking the correctness of the estimate of fluctuations of intensities, described by Σ_F than for getting information on PSFs. No significant deviation of χ^2 values from the expected behavior is visible in Table II.

The χ^2 values corresponding to $J_{L_j} = 3/2$ clearly show that with the exception of the PSF shape of model D, which is derived from $(d, p\gamma\gamma)$ data itself, there is no above-introduced PSF model which can satisfactorily describe data from $E_i =$ 6–7 MeV. As a result we decided to discuss the acceptability of tested models separately for two regions of E_γ.

1. Results for $E_\gamma < 4$ MeV

Probably the most interesting is the $E_\gamma \lesssim$ 3–4 MeV region, where a significant PSF decrease with E_γ has been reported from Oslo data. This region can be probed by our $E_i =$ 3–5 MeV data; higher E_i cannot be used owing to lack of experimental points for low E_γ. Expected relative fluctuations of individual intensities $N_{L_j}(E_i, E_\gamma)$, described by Σ_F, are significant at these excitation energies and may be bigger than experimental uncertainties.

The χ^2 values listed in Table II imply that no strong restrictions on PSFs models can be made using the standard χ^2-based analysis. Using the χ^2 criterion, data at $E_\gamma < 4$ MeV are fully consistent with all B-type, as well as A, $A^\dagger$, and D, models. In addition, a constant PSF (model E) and an increasing PSF at these E_γ, as given by the low-E_γ dependence for model C, are still acceptable on high probability levels of 10% and 5%, respectively. Moreover, as mentioned above, the Σ_F values listed in Table II likely underestimate the real ones allowing consistency of even a broader range of PSF models. Significantly different χ^2 values for A-type models also indicate that there is a sensitivity to the shift Δ in the GLO model. The noted limited sensitivity makes also a prospective determination of c (or σ_c), as proposed in Sec. III A 2, very difficult using this E_γ region.

TABLE III. Significance levels for rejection of various PSF models, specified in the second row, using the Cox approach [33] with respect to model B. Two NLD models, specified in the first column, and two options for fluctuation of $\sigma_{kJ,(d,p)}(E_i)$, specified in the second column, were adopted; see the main text for details.

NLD	$\sigma_{kJ,(d,p)}(E_i)$ fluctuation	Significance level (%) A	$A^\dagger$	B^*	$B^\dagger$	C	D	E
BSFG	None	98.8	98.4	99.8	99.2	99.998	85	99.97
BSFG	PTD	96.1	96.3	99.1	97.6	99.95	78	99.85
CT	None	97.3	97.4	99.6	98.5	99.98	82	99.94
CT	PTD	94.5	95.5	98.3	96.1	99.83	76	99.6

Nevertheless, more powerful approaches can be invoked for testing a pair of competing hypotheses if one of them is correct, notably the Cox test of linear regression models [33]. With this approach even seemingly miniscule differences in χ^2 values, $\Delta\chi^2_{\rm exp} = \chi^2_{H_1} - \chi^2_{H_0}$, obtained with two hypotheses (models) H_0 and H_1 for the same set of experimental data, may allow for rejection of one of them in favor of the other at high significance level. Motivated by the Cox approach, we tested the compatibility of a $\Delta\chi^2_{\rm exp}$ value with the distribution expected for this quantity under the assumption that H_0 is valid.

In practice, we considered 28 pairs (H_0, H_1). In all of them H_0 was represented by one of 14 combinations of the PSF and LD models in conditions of presence or absence of the Porter-Thomas fluctuations for $\sigma_{kJ,(d,p)}(E_i)$, as specified in Table III and Sec. III B. For H_1 we chose the model B, as the sum of χ^2 values from experimental data reaches the lowest value among all tested PSF models. For each pair we simulated 10^6 artificial data sets based on validity of each choice of hypothesis H_0. This enabled us to construct the expected distributions of $\Delta\chi^2$. Experimental uncertainties were taken into account during simulations. The same normalization procedure as that used for the experimental data, was applied to each artificial data set. Only transitions with $E_\gamma < 4$ MeV were used in the analysis. At least two transitions with these energies were found for all J_{L_j} from $E_i =$ 3–4 MeV and also for $J_{L_j} = 3/2$ from $E_i = 5$ MeV.

Having the constructed distributions of $\Delta\chi^2$, we determined statistical significance levels for rejection of each of the considered PSF and LD model combination in favor of PSF model B. These results are listed in Table III.

As discussed above, the actual distribution of $\sigma_{kJ,(d,p)}(E_i)$, as well as the actual number of levels in the region near E_i contributing to the feeding of low-lying levels is not precisely known, and could differ from any assumption used in Table III. Nonetheless, the listed probabilities for rejection serve as an illustration of the power of the used Cox approach. The highest (smallest) significance levels in each column of the

table correspond to the smallest (highest) values of Σ_F. The combination of the BSFG NLD for number of levels with no fluctuation of $\sigma_{kJ,(d,p)}(E_i)$ likely gives unrealistically low Σ_F, while other combinations should be closer to reality.

The values listed in Table III indicate that several tested models cannot be rejected at high significance levels; the significance levels corresponding to rejection of a model at standard 2σ and 3σ levels are 97.72% and 99.87%, respectively. Only a constant PSF (model E) or a PSF which is a slowly increasing function of E_γ (model C) can be rejected with really high confidence using the Cox approach. Moreover, as the Cox approach tests a pair of competing hypotheses the meaning of significance levels is problematic if none of the hypotheses is correct. For illustration, if we test the significance level for rejection assuming validity of one of the models A—the model reproducing coincidence (n,γ) data—and E, then the constant PSF (model E) can be rejected at the significance level ranging from 97% [for PTD fluctuation of $\sigma_{kJ,(d,p)}(E_i)$ and the CT NLD model] to 99.4% [no fluctuation of $\sigma_{kJ,(d,p)}(E_i)$ and the BSFG NLD model].

To summarize the discussion, it seems difficult to draw definite conclusions on the PSF E_γ dependence for $E_\gamma < 4$ MeV from the data measured in the ^{94}Mo$(d,p\gamma\gamma)^{95}$Mo reaction. According to us, the appropriate statement is that a PSF decrease with E_γ at $E_\gamma \approx$ 1–3 MeV is preferred, but the experimental $(d,p\gamma\gamma)$ data cannot unambiguously decide if the shape is more similar to that proposed from the Oslo-type experiment or to predictions from the combination of the GLO model for $E1$ PSF and SP and SF models for $M1$ PSF, preferred by (n,γ) data, which exhibits a less steep decrease of PSF with E_γ.

2. *Results for $E_\gamma > 4$ MeV*

The PSF is expected to rise with E_γ at $E_\gamma > 4$ MeV. This E_γ region can be probed with data for $E_i \gtrsim 5$ MeV, where expected fluctuations Σ_F are significantly smaller than experimental errors. As a result, the acceptability of individual models depends only weakly on expected fluctuation properties of $\sigma_{kJ,(d,p)}(E_i)$, as well as on NLD models used in estimating Σ_F.

As evident from Table II, agreement of experimental points for $J_{L_j} = 3/2$ levels with all A-, B-, and C-type model combinations is poor for $E_\gamma \gtrsim 5$ MeV. Considering the χ^2 values for $E_i =$ 6–7 MeV for $J_{L_j} = 3/2$, all these models can be rejected at a significance level of at least 99.93%, even if $\sigma_{kJ,(d,p)}(E_i)$ fluctuates according to the PTD. Figures 2 and 3 indicate that the E_γ dependence of the PSFs must be steeper than predicted by any of these model combinations; it is to be similar to that in model D.

According to our knowledge, such a steep E_γ dependence of the PSF has never been observed in any previous experiment exploiting a nuclear reaction with a hadronic probe. Model D allows for perfect matching of the PSF from (γ,n) data, which are above S_n usually well described with a Lorentzian shape (C^* model), with the absolute PSF values at $E_\gamma \lesssim 5$ MeV predicted by the GLO model or by models based on Oslo data. The model also reasonably reproduces the total radiation width of neutron resonances; see Table IV and Sec. III C 3.

TABLE IV. Total radiation width of neutron resonances, $\Gamma_{T,\mathrm{res}}$, predicted by tested PSF models in combination with the BSFG NLD model. Fluctuations in simulations come from Porter-Thomas fluctuations of individual transition intensities. The experimental value for p-wave resonances comes from a mixture of $1/2^-$ and $3/2^-$ resonances. Uncertainties in experimental values correspond to error of the mean and do not reflect the fluctuations between individual widths.

Model	$\Gamma_{T,\mathrm{res}}$ (meV)		
	$1/2^+$	$1/2^-$	$3/2^-$
A	150(15)	190(25)	170(20)
B[a]	80(10)	140(30)	110(20)
B[b]	90(10)	120(30)	110(20)
B^*[a]	90(10)	210(60)	160(30)
B^*[b]	120(20)	180(50)	150(30)
$B^\dagger$[a]	80(10)	250(90)	180(50)
$B^\dagger$[b]	120(20)	210(70)	160(40)
C	250(30)	510(120)	410(70)
C^*	400(40)	680(150)	570(90)
D[a]	85(10)	240(80)	180(50)
D[b]	120(20)	220(70)	170(40)
Experiment [22]	128(9)	188(10)	

[a]PSFs assumed to be only of $E1$ type.
[b]Ratio $f_{(E1)}(E_\gamma)/f_{(M1)(E_\gamma)} = 4$ for all E_γ (see text for details).

We would like to note here that (n,γ) data in neighboring Mo nuclei analyzed in Refs. [6–8] are not very sensitive to PSFs at $E_\gamma \gtrsim 5-6$ MeV, and the precise E_γ dependence of the PSF can hardly be determined from an analysis of primary transition intensities owing to their restricted number in the Mo mass region. The PSF slope from ELBE data (model C) is similar to that of model D for $E_\gamma \approx 4-6$ MeV, but there is a significant difference between these two PSF models at higher E_γ. Although the steepness of $(d,p\gamma\gamma)$ data, together with the shape of $\sigma_{\gamma T}$ just above S_n, might indicate that we observe a pygmy resonance situated near 8 MeV, the difference in position of the resonance maximum between $(d,p\gamma\gamma)$ and the ELBE data does not allow to make any definite conclusions on the actual PSF shape in the $E_\gamma =$ 5–9-MeV region.

The PSF slope for $E_\gamma =$ 5–7 MeV, obtained from $(d,p\gamma\gamma)$ data, might also be used for fixing the PSF E_γ dependence (via constant c or σ_c) in the Oslo method. Higher PSF slopes in this E_γ region with respect to those from Refs. [4,24] would reduce the low-E_γ PSF enhancement deduced from Oslo experiments. The E_γ dependence of the PSF at $E_\gamma \lesssim 3.5$ MeV would then be very similar to that predicted with the A model combination from $E_i \approx 3.5$ MeV. The PSF corresponding to model B multiplied by a factor $e^{0.25E_\gamma}$, which reasonably reproduces the E_γ dependence of $(d,p\gamma\gamma)$ data for $E_\gamma \gtrsim 5$ MeV, is, after a renormalization, plotted in Fig. 3 and labeled as $B^\dagger$. The acceptability of this model at low E_γ is similar to the acceptability of model A; see values in Tables II and III. We have to admit that the proposed change of PSF slope would require a significantly different spin dependence of NLD in the neutron resonance region from that used in Refs. [4,24,34]. Specifically, the total NLD derived from Oslo data corresponding to PSF model $B^\dagger$ would be higher by a

factor of about six in the resonance region compared to the original NLD from Ref. [34]. The fraction of the total NLD, represented by observed neutron resonances, would then be smaller by the same factor than the fraction assumed in Ref. [4] (or σ_c^2 would be higher by a similar factor).

3. Total radiation width

Predicted values of total radiation width of neutron resonances $\Gamma_{T,\mathrm{res}}$ from DICEBOX simulations are listed in Table IV for all tested models. As $\Gamma_{T,\mathrm{res}}$ depends on the absolute PSF normalization and the number of levels to which resonances can decay [see Eq. (7)], these quantities can be used as a partial check of correctness of the PSF absolute normalization. The $\Gamma_{T,\mathrm{res}}$ values presented in Table IV were obtained with the absolute normalization of PSF models, as shown in Figs. 2 and 3 and with the BSFG model of NLD. If the CT model of NLD is used, $\Gamma_{T,\mathrm{res}}$ values are smaller by about 30%–40%, slightly depending on the PSF model combination. The uncertainties in predicted $\Gamma_{T,\mathrm{res}}$ come from fluctuations of individual partial radiation widths according to the PTD.

Predicted $\Gamma_{T,\mathrm{res}}$ for resonances with different parity depends significantly on the XL makeup of the PSF at $E_\gamma \gtrsim 5$ MeV, owing to the dominance of levels with positive parity at low excitation energies. This influence is illustrated in Table IV for several models. The two calculated $\Gamma_{T,\mathrm{res}}$ values correspond to (i) all strength of $E1$ type and (ii) $f_{(E1)}(E_\gamma)/f_{(M1)}(E_\gamma) = 4$ for all E_γ. The ratio in the latter option corresponds to results from an analysis of primary transitions in (n,γ) reaction in the Mo region [14] and $\Gamma_{T,\mathrm{res}}$ predicted with this ratio are thus more appropriate. In general, transfer of some strength from $E1$ to $M1$ for $E_\gamma \gtrsim 5$ MeV increases (decreases) $\Gamma_{T,\mathrm{res}}$ from positive- (negative)-parity resonances. Sensitivity of $\Gamma_{T,\mathrm{res}}$ to the XL makeup at lower E_γ is much smaller as the number of levels with both parities is expected to be similar at higher excitation energies; a parity-independent NLD was assumed above 2.1 MeV in simulations.

Good reproduction of absolute experimental $\Gamma_{T,\mathrm{res}}$ values with predictions based on a combination of PSF model D, with $f_{(E1)}(E_\gamma)/f_{(M1)}(E_\gamma) = 4$, and BSFG NLD indicates that the absolutization of $(d,p\gamma\gamma)$ experimental data is adequate in Fig. 3, where the data are normalized to model D. Reproduction of $\Gamma_{T,\mathrm{res}}$ for PSF model D in combination with the CT NLD model would require a multiplication of the PSF model, or $(d,p\gamma\gamma)$ experimental data, by a factor of about 1.3; the data, although closer, would still be somewhat lower than the ELBE (γ,γ') data.

IV. SUMMARY

A detailed discussion of the relation between photon strength functions and experimentally observed E_γ dependence of intensities of γ transitions, feeding low-lying levels from levels at higher excitation energies produced in (d,p) reaction, is presented. The E_γ dependence of observed intensities, reduced by E_γ^3, from selected regions of initial energies is, in general, proportional to a nontrivial combination of $E1$ and $M1$ PSFs. When assessing the magnitude of the contributions of each transition type, we found commanding influence of the ratio of total radiation widths for levels with different parity at the same initial excitation energy. The proportionality of reduced intensities to $f_{(E1)}(E_\gamma) + f_{(M1)}(E_\gamma)$ seems to be approximately satisfied for γ transitions from levels at high excitation energies of ^{95}Mo produced in the ^{94}Mo$(d,p\gamma\gamma)^{95}$Mo reaction [17].

Assuming the proportionality, we compared the consistency of several PSF E_γ dependencies with experimental data. Unfortunately, a fully correct quantitative comparison appears to be difficult, especially owing to uncertainties in fluctuations of the cross section for the production of individual levels in the (d,p) reaction. Despite this uncertainty, some general conclusions can be made.

The standard χ^2 test for the comparison of experimental data with model predictions does not allow to make strong constraints on the E_γ dependence of the PSF at $E_\gamma \lesssim 4$ MeV. The test cannot unambiguously decide whether the PSF is a strongly decreasing function of E_γ at $E_\gamma \lesssim 3$ MeV—as proposed from ^{3}He-induced reactions—or a slowly increasing function of E_γ.

Stronger restrictions on acceptable models can be applied using more powerful statistical tests by comparing the validity of competing hypotheses, assuming correctness of one of them. These statistical tests indicate that the PSF in ^{95}Mo is likely a decreasing function of E_γ at $E_\gamma \approx 1$–3 MeV. Nevertheless, even these tests are unable to decide if the decrease rather follows the PSF E_γ dependence derived from Oslo experiments or the dependence predicted by the temperature-dependent GLO model of $E1$ PSF in combination with the single-particle and spin-flip models of $M1$ PSF, reproducing data from (n,γ) reactions, at these E_γ. Additional experimental data on the PSFs are highly desired to get more precise information on the E_γ dependence of the PSF in this E_γ region.

At higher E_γ, data from the ^{94}Mo$(d,p\gamma\gamma)^{95}$Mo reaction indicate that the E_γ dependence of the PSF is steeper than predicted by any of the tested models which are based on results from nuclear reactions induced by hadronic probes. The PSF shape seems to be similar at $E_\gamma \approx 4$–6 MeV to results from (γ,γ') measurements but with a significant deviation at $E_\gamma \gtrsim 6$ MeV. The steep PSF from the ^{94}Mo$(d,p\gamma\gamma)^{95}$Mo reaction for $E_\gamma \approx 5$–7 MeV seems to nicely match absolute PSF values above S_n from (γ,n) data with the PSF values proposed from Oslo or (n,γ) data at $E_\gamma \lesssim 5$ MeV. Independent experimental confirmation of the PSF shape in this region would also be highly appreciated.

ACKNOWLEDGMENTS

The work was supported from Grant No. 13-07117S of the Czech Science Foundation. Part of this work was supported by the National Research Foundation of South Africa under Grant No. 92789.

[1] Report of the Nuclear Physics and Related Computational Science R&D for Advanced Fuel Cycles Workshop, DOE Offices of Nuclear Physics and Advanced Scientific Computing Research, August 2006.

[2] C. Sneden, J. J. Cowan, and R. Gallino, Annu. Rev. Astron. Astrophys. **46**, 241 (2008).

[3] G. J. Mathews and R. A. Ward, Rep. Prog. Phys. **48**, 1371 (1985).

[4] M. Guttormsen, R. Chankova, U. Agvaanluvsan, E. Algin, L. A. Bernstein, F. Ingebretsen, T. Lonnroth, S. Messelt, G. E. Mitchell, J. Rekstad, A. Schiller, S. Siem, A. C. Sunde, A. Voinov, and S. Odegard, Phys. Rev. C **71**, 044307 (2005).

[5] A. Schiller, L. Bergholt, M. Guttormsen, E. Melby, J. Rekstad, and S. Siem, Nucl. Instrum. Methods Phys. Res., Sect. A **447**, 498 (2000).

[6] S. A. Sheets, U. Agvaanluvsan, J. A. Becker, F. Bečvář, T. A. Bredeweg, R. C. Haight, M. Jandel, M. Krtička, G. E. Mitchell, J. M. O'Donnell, W. Parker, R. Reifarth, R. S. Rundberg, E. I. Sharapov, J. L. Ullmann, D. J. Vieira, J. B. Wilhelmy, J. M. Wouters, and C. Y. Wu, Phys. Rev. C **79**, 024301 (2009).

[7] M. Krtička, F. Bečvář, I. Tomandl, G. Rusev, U. Agvaanluvsan, and G. E. Mitchell, Phys. Rev. C **77**, 054319 (2008).

[8] C. L. Walker, M. Krtička, B. Baramsai, F. Bečvář, T. A. Bredeweg, A. Chyzh, R. C. Haight, M. Jandel, J. Kroll, G. E. Mitchell, J. M. O'Donnell, R. S. Rundberg, J. L. Ullmann, S. Valenta, and J. B. Wilhelmy, Phys. Rev. C **92**, 014324 (2015).

[9] G. Rusev, R. Schwengner, F. Donau, M. Erhard, E. Grosse, A. R. Junghans, K. Kosev, K. D. Schilling, A. Wagner, F. Becvar, and M. Krticka, Phys. Rev. C **77**, 064321 (2008).

[10] C. Romig, J. Beller, J. Glorius, J. Isaak, J. H. Kelley, E. Kwan, N. Pietralla, V. Y. Ponomarev, A. Sauerwein, D. Savran, M. Scheck, L. Schnorrenberger, K. Sonnabend, A. P. Tonchev, W. Tornow, H. R. Weller, A. Zilges, and M. Zweidinger, Phys. Rev. C **88**, 044331 (2013).

[11] G. Rusev, C. T. Angell, R. Beyerd, F. Dönaud, M. Erhardd, E. Grossed, S. L. Hammond, A. L. Hutchesona, S. Frauendorfd, A. R. Junghans, H. J. Kawowski, J. H. Kelley, J. Klugd, K. Kosevd, E. Kwana, C. Naird, N. Nikolovd, K.D. Schilling, R. Schwengnerd, A. P. Toncheva, W. Tornowa, and A. Wagnerd, *Application of Accelerators in Research and Industry: 20th International Conference*, AIP **1099**, 799 (2009).

[12] J. Kopecky and M. Uhl, Phys. Rev. C **41**, 1941 (1990), and references therein.

[13] M. Krtička and F. Becvář, EPJ Web Conf. **2**, 03002 (2010).

[14] J. Kopecky, Gamma-Ray Strength Functions, Handbook for Calculations of Nuclear Reaction Data-Reference Input Parameter Library, IAEA-TECDOC-1034, IAEA, Vienna, 1998, p. 97; directory GAMMA on the web site http://www-nds.iaea.org/ripl/

[15] E. Litvinova and N. Belov, Phys. Rev. C **88**, 031302 (2013).

[16] R. Schwengner, S. Frauendorf, and A. C. Larsen, Phys. Rev. Lett. **111**, 232504 (2013).

[17] M. Wiedeking, L. A. Bernstein, M. Krtička, D. L. Bleuel, J. M. Allmond, M. S. Basunia, J. T. Burke, P. Fallon, R. B. Firestone, B. L. Goldblum, R. Hatarik, P. T. Lake, I. Y. Lee, S. R. Lesher, S. Paschalis, M. Petri, L. Phair, and N. D. Scielzo, Phys. Rev. Lett. **108**, 162503 (2012).

[18] S. R. Lesher, L. Phairc, L.A. Bernsteina, D.L. Bleuela, J.T. Burkea, J.A. Churcha, P. Fallonc, J. Gibelinc, N.D. Scielzoa, and M. Wiedekinga, Nucl. Instrum. Methods Phys. Res., Sect. A **621**, 286 (2010).

[19] G. A. Bartholomew *et al.*, Adv. Nucl. Phys. **7**, 229 (1973).

[20] F. Bečvář, Nucl. Instrum. Methods Phys. Res., Sect. A **417**, 434 (1998).

[21] M. Wiedeking, M. Krtička, L. A. Bernstein, J. M. Allmond, M. S. Basunia, D. L. Bleuel, J. T. Burke, B. H. Daub, P. Fallon, R. B. Firestone, B. L. Goldblum, R. Hatarik, P. T. Lake, A. C. Larsen, I.-Y. Lee, S. R. Lesher, S. Paschalis, M. Petri, L. Phair, N. D. Scielzo, and A. Volya, Phys. Rev. C **93**, 024303 (2016).

[22] S. F. Mughabghab, *Atlas of Neutron Resonances* (Elsevier, Amsterdam, 2006).

[23] A. J. Koning *et al.*, in *Nuclear Data for Science and Technology*, edited by O. Bersillon *et al.*, (EDP Sciences, London, 2008), p. 211; see also http://www.talys.eu

[24] A. C. Larsen and S. Goriely, Phys. Rev. C **82**, 014318 (2010).

[25] S. S. Dietrich and B. L. Berman, At. Data Nucl. Data Tables **38**, 199 (1988).

[26] T. von Egidy and D. Bucurescu, Phys. Rev. C **80**, 054310 (2009).

[27] T. von Egidy, H. H. Schmidt, and A. N. Behkami, Nucl. Phys. A **481**, 189 (1988).

[28] A. C. Larsen, N. Blasi, A. Bracco, F. Camera, T. K. Eriksen, A. Gorgen, M. Guttormsen, T. W. Hagen, S. Leoni, B. Million, H. T. Nyhus, T. Renstrom, S. J. Rose, I. E. Ruud, S. Siem, T. Tornyi, G. M. Tveten, A. V. Voinov, and M. Wiedeking, Phys. Rev. Lett. **111**, 242504 (2013).

[29] D. M. Brink, Ph.D. thesis, Oxford University, 1955.

[30] H. Utsunomiya, S. Goriely, T. Kondo, C. Iwamoto, H. Akimune, T. Yamagata, H. Toyokawa, H. Harada, F. Kitatani, Y. W. Lui, A. C. Larsen, M. Guttormsen, P. E. Koehler, S. Hilaire, S. Péru, M. Martini, and A. J. Koning, Phys. Rev. C **88**, 015805 (2013).

[31] C. E. Porter and R. G. Thomas, Phys. Rev. **104**, 483 (1956).

[32] S. K. Basu, G. Mukherjee, and A. A. Sonzogni, Nucl. Data Sheets **111**, 2555 (2010).

[33] D. R. Cox, J. R. Stat. Soc. Ser. B **24**, 406 (1962).

[34] R. Chankova, A. Schiller, U. Agvaanluvsan, E. Algin, L. A. Bernstein, M. Guttormsen, F. Ingebretsen, T. Löonnroth, S. Messelt, G. E. Mitchell, J. Rekstad, S. Siem, A. C. Larsen, A. Voinov, and S. Ødegård, Phys. Rev. C **73**, 034311 (2006).